Interaction of Myelin Basic Protein with Actin in the Presence of Dodecylphosphocholine Micelles

ARTICLE *in* BIOCHEMISTRY · AUGUST 2010

Impact Factor: 3.02 · DOI: 10.1021/bi100308d · Source: PubMed

3 AUTHORS, INCLUDING:

Vladimir V Bamm
University of Guelph
37 PUBLICATIONS **534** CITATIONS
SEE PROFILE

Mumdooh A M Ahmed
Helmholtz Centre for Infection Research
18 PUBLICATIONS **347** CITATIONS
SEE PROFILE

BIOCHEMISTRY
including biophysical chemistry & molecular biology
Article

Biochemistry **2010,** *49,* 6903–6915 6903
DOI: 10.1021/bi100308d

Interaction of Myelin Basic Protein with Actin in the Presence of Dodecylphosphocholine Micelles[†]

Vladimir V. Bamm,[‡,#] Mumdooh A. M. Ahmed,[§,∥,⊥,#] and George Harauz*[,‡,∥]

[‡]*Department of Molecular and Cellular Biology,* [§]*Department of Physics, and* [∥]*Biophysics Interdepartmental Group, University of Guelph, 50 Stone Road East, Guelph, Ontario N1G 2W1, Canada, and* [⊥]*Department of Physics, Faculty of Science at Suez, Suez-Canal University, Suez, Egypt.* [#]*These authors contributed equally to this work.*

Received March 2, 2010; Revised Manuscript Received June 28, 2010

ABSTRACT: The 18.5 kDa myelin basic protein (MBP), the most abundant splice isoform in human adult myelin, is a multifunctional, intrinsically disordered protein that maintains compact assembly of the myelin sheath in the central nervous system. Protein deimination and phosphorylation are two key posttranslational modifications whose balance determines local myelin microdomain stability and function. It has previously been shown that MBP in solution causes both polymerization of G-actin to F-actin and bundling of the microfilaments, and binds them to a negatively charged membrane. However, the binding parameters, and the roles of different possible interacting domains of membrane-associated MBP, have not yet been investigated. Here, we compared the interaction of unmodified (rmC1) and pseudodeiminated (rmC8) recombinant murine MBP (full-length charge variants), and of two terminal deletion variants (rmΔC and rmΔN), with actin in the presence of DPC (dodecylphosphocholine) to mimic a membrane environment. Our results show that although both charge variants polymerized and bundled actin, the maximal polymerization/bundling due to rmC1 occurred at a lower molar ratio compared to rmC8. In the presence of DPC, rmC1 appeared to be more active than rmC8 in its ability to polymerize and bundle actin, and the binding affinity of both charge variants to G-actin became higher. Moreover, of the two deletion variants studied in the presence of DPC, the one lacking the C-terminal domain (rmΔC) was more active compared to the variant lacking the N-terminal domain (rmΔN) but exhibited weaker binding to actin. Thus, whereas the N-terminal domain of MBP can be more important for the MBP's actin polymerization activity and membrane-association, the C-terminal domain can regulate its interaction with actin.

The myelin basic protein (MBP)[1] family of proteins has been known as central nervous system (CNS) self-antigens, which can induce experimental autoimmune encephalomyelitis in mice, a model for the inflammatory component of demyelinating diseases such as multiple sclerosis (MS) (*1*). The most studied candidate autoantigen in MS is the "classic" 18.5 kDa MBP isoform that originates from transcription start site 3 of the gene (*2*). This isoform is preponderant in the adult human CNS, where it maintains the compact multilamellar myelin assembly by adhesion of the apposing cytoplasmic leaflets of the oligodendrocyte membrane (*3*, *4*).

The predominant 18.5 kDa isoform (from now on referred to as MBP for simplicity) belongs to the class of intrinsically disordered proteins, many of which are multifunctional and participate in signal transduction (*5*, *6*). Due to its intrinsically disordered nature, the structural flexibility of MBP enables it to interact with many different partners in the CNS, including with calcium-activated calmodulin (Ca-CaM), actin, tubulin, SH3-binding proteins, and divalent metal cations (*7*−*11*). Unmodified MBP is an extremely positively charged protein (+19 at neutral pH) and exists as a number of charge components or isomers due to a wide variety of posttranslational modifications, such as methylation, phosphorylation, and deimination (*12*). The "dynamic molecular barcode" of these combinatorial modifications modulates the interaction of MBP with the membrane and with other ligands (*13*, *14*).

Though originally MBP was considered to be simply a structural component of myelin, many additional investigations have demonstrated that MBP is a multifunctional protein. It has been shown that MBP *in vitro* interacts with cytoskeletal proteins (*7*−*9*, *15*−*17*). Specifically, in solution, it causes polymerization of G-actin to F-actin and bundling of the microfilaments. This function is modulated by posttranslational modifications of MBP, primarily phosphorylation and deimination, and reversed by binding of

[†]This work was supported by the Canadian Institutes of Health Research (CIHR, MOP 74468 to G.H.). V.V.B. was the recipient of a postdoctoral fellowship from the Multiple Sclerosis Society of Canada, and M.A.M.A. was the recipient of a doctoral studentship from the Ministry of Higher Education and Scientific Research of Egypt.

*To whom correspondence should be addressed at the Department of Molecular and Cellular Biology, University of Guelph. E-mail: gharauz@uoguelph.ca. Fax: 519-837-1802. Telephone: 519-824-4120 ext 52535.

[1]Abbreviations: rmΔC, rmMBP(A1-G105W-His_6), lacking the C-terminal domain and with G105W substitution; rmΔN, rmMBP(D57-R168-Leu-Glu-His_6), lacking the N-terminal domain; CNS, central nervous system; EPR, electron paramagnetic resonance spectroscopy; DPC, dodecylphosphocholine; F-actin, filamentous actin; G-actin, globular actin; IPTG, isopropyl β-D-thiogalactopyranoside; IDP, intrinsically disordered protein; MBP, myelin basic protein; MS, multiple sclerosis; NMR, nuclear magnetic resonance; rmMBP, 18.5 kDa recombinant murine MBP (A1-R168-Leu-Glu-His_6); rmC1, recombinant murine MBP, unmodified C1 charge component; rmC8, recombinant murine MBP, pseudodeiminated C8 charge component; SDS, sodium dodecyl sulfate; SDS−PAGE, sodium dodecyl sulfate−polyacrylamide gel electrophoresis; Tris, tris(hydroxymethyl)aminomethane.

Published on Web 07/02/2010

Ca-CaM (*8*, *16*−*18*). Moreover, MBP has been shown to interact simultaneously with actin and lipid vesicles, thus supporting its suggested role in the organization of the actin cytoskeleton and in tethering it to the inner leaflet of the oligodendrocyte membrane (*16*). In oligodendrocytes cultured from the *shiverer* mouse (which lacks MBP), actin filaments appeared to be disorganized, and the cell processes were smaller than normal with a larger cell body (*19*−*21*). Altogether, these diverse observations suggest that the interaction of MBP with cytoskeletal proteins is crucial for oligodendrocyte function.

The interaction of MBP with actin is mostly electrostatic and has been shown to be inhibited by increasing salt concentration and by two posttranslational modifications resulting in the decrease of the net positive charge of MBP (phosphorylation and deimination) (*8*, *17*, *18*). Since MBP−lipid interaction involves induced ordered secondary structure (primarily α-helical) (*22*−*30*) and since different segments of the MBP polypeptide chain are embedded in the lipid bilayer, it is expected that some of the positively charged residues of the membrane-associated protein will be masked or less accessible for interactions with other partners. Therefore, the interaction of MBP with actin is expected to be different in aqueous solution and in a lipidic environment; particularly, the stoichiometry and the strength of binding can be altered.

In this paper, we have studied the interaction parameters (polymerization and bundling) of recombinant murine MBP (rmMBP, first the unmodified rmC1 variant) and actin in the presence of dodecylphosphocholine (DPC) micelles (detergent with critical micelle concentration of 1 mM) as a membrane-mimetic condition that can be studied using solution spectroscopic approaches (*27*). In previous studies, it has been shown that one molecule of full-length MBP interacts with 200 molecules of DPC (*22*, *31*). Since one DPC micelle contains 40−60 detergent molecules, this means that each MBP binds about four DPC micelles. Moreover, in the same study the investigators showed that several MBP-derived peptides bound at least 100 DPC molecules or two micelles (*31*). These early studies were performed on MBP purified from brain and comprising heterogeneous mixtures of many posttranslationally modified components. In the present study, we use well-defined recombinant MBP variants, starting with the unmodified 18.5 kDa rmC1 protein. We have also determined the effects of charge loss in MBP (using pseudodeiminated rmMBP variant, rmC8, where five Arg and one Lys were substituted by Gln) (*32*), and deletion of either the N-terminal or the C-terminal domain (rmΔN and rmΔC, respectively) (*33*), on the actin-binding affinity and stoichiometry in the presence of DPC. Our results show that, in the presence of DPC, rmC1 appeared to be more active than rmC8 in its ability to polymerize and bundle actin, and their binding to G-actin became more specific with higher affinity. Of the two terminal deletion variants, the rmΔC protein lacking the C-terminal domain was more active than the rmΔN variant lacking the N-terminal domain, which, however, exhibited higher affinity to actin. We conclude that, whereas the N-terminal domain plays a more significant role in the actin polymerization and bundling activity of MBP, the C-terminal domain could be more important in the regulation of that activity.

MATERIALS AND METHODS

Materials. Electrophoresis grade acrylamide, ultrapure Tris base, and ultrapure Na_2EDTA were purchased from ICN Biomedicals (Costa Mesa, CA). Other chemicals were of reagent grade and were acquired from either Fisher Scientific (Unionville, Ontario, Canada) or Sigma-Aldrich (Oakville, Ontario, Canada). The Ni^{2+}-NTA (nitrilotriacetic acid) agarose beads were purchased from Qiagen (Mississauga, Ontario, Canada). For uniform labeling of proteins for NMR spectroscopy, the stable isotopic compounds D_2O, $^{15}NH_4Cl$, and [$^{13}C_6$]glucose were obtained from Cambridge Isotope Laboratories (Andover, MA).

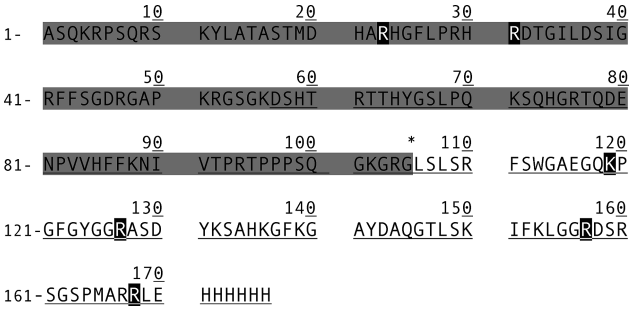

FIGURE 1: Sequences of rmMBP variants. The recombinant murine rmMBP-C1 charge variant (rmC1) has an LE linker and His_6 tag at the C-terminus of the protein. Residues denoted with white letters "R" and "K" in the black square indicate the positions where the five R and one K in rmC1 were point-substituted by Q to create pseudodeiminated rmMBP (rmC8) (*32*). Parts of the sequence highlighted with gray color and underlined indicate the polypeptide sequences of rmΔC and rmΔN variants, respectively (*33*). The rmΔN variant has an N-terminal Met and LE His_6 tag. In the rmΔC variant, the N-terminal Met is missing, and another point mutation of G105W was introduced (marked with an asterisk), and a His_6 tag was added at the C-terminus.

Expression and Purification of rmMBP. The unmodified 18.5 kDa recombinant murine MBP isoform (rmC1), its pseudodeiminated form (rmC8, where five Arg and one Lys were substituted by Gln to mimic citrulline), and two deletion variants (rmΔC and rmΔN) (Figure 1) were expressed in *Escherichia coli* BL21-CodonPlus(DE3)-RP cells (Stratagene, La Jolla, CA) and purified by nickel-affinity chromatography, followed by ion-exchange chromatography to remove minor contaminating material, as previously described (*32*−*34*). Protein eluate from the column was dialyzed (using tubing with M_r cutoff 6000−8000 Da for full-length proteins and 3500 Da for the deletion variants) twice against 2 L of buffer (50 mM Tris-HCl, pH 7.4, 250 mM NaCl), twice against 2 L of 100 mM NaCl, and finally four times against 2 L of ddH_2O. Protein concentration was determined by measuring the absorbance at 280 nm, using the extinction coefficients $\varepsilon = 0.667$ L g^{-1} cm^{-1}, $\varepsilon = 0.672$ L g^{-1} cm^{-1}, $\varepsilon = 0.674$ L g^{-1} cm^{-1}, and $\varepsilon = 0.885$ L g^{-1} cm^{-1} for rmC1, rmC8, rmΔC, and rmΔN, respectively (as calculated by SwissProt for protein in 6.0 M guanidine hydrochloride, 0.02 M phosphate buffer, pH 6.5, Table 1). Purity of the protein preparations was routinely assayed by SDS−polyacrylamide gel electrophoresis (SDS−PAGE) (*35*).

Purification of Actin from Chicken Muscle. Chicken muscle acetone powder was prepared, and actin was extracted from 8 g of it at a time as described in detail elsewhere (*36*). The purity of actin was checked using MALDI-TOF mass spectrometry, supported by SDS−PAGE, and it was clear that no further purification steps were required. Protein concentration was determined by measuring the absorbance at 280 nm, using the extinction coefficient $\varepsilon = 0.62$ L g^{-1} cm^{-1}. Actin that was suspended in G buffer (2 mM Tris, pH 8.0, 0.2 mM ATP, 0.2 mM $CaCl_2$, and 0.2 mM 2-mercaptoethanol) was aliquoted into 1.5 mL microfuge tubes, flash-frozen in liquid nitrogen, and stored at −80 °C. The pyrene labeling of actin was performed as previously published (*37*).

Table 1: Calculated Physicochemical Parameters of rmMBP Charge and Deletion Variants[a]

variant	M_r, Da	no. of residues	theoretical pI/net charge	calcd ε_{280}, L g^{-1} cm^{-1}
rmC1	19421.5	176	11.00/+19	0.667
rmC8	19281.2	176	10.35/+13	0.672
rmΔN	13401.8	121	10.47/+11	0.885
rmΔC	12582.9	111	11.39/+12	0.674

[a]The parameters were calculated for the MBP variants based on amino acid sequence using the ProtParam software tool available at the website http://expasy.ch.

Actin Polymerization Assay. Actin polymerization was followed by measuring an increase in fluorescence intensity of pyrene-labeled actin employing an automated microplate fluorescence reader (Polarstar Omega; BMG Labtech GmbH, Offenburg, Germany), using a 367-10 nm filter for the excitation channel and a 405-10 nm filter for the emission channel. The stock of 50 μM G-actin was prepared in G buffer by mixing pyrene-labeled actin with unlabeled actin to a final labeled proportion of 5%, and 10 μL of actin was added to each well followed by an additional volume of G buffer, calculated to give a final volume of 100 μL after addition of rmMBP. Stocks of rmMBP variants (rmC1, rmC8, rmΔC, and rmΔN) were also prepared in G buffer at a concentration of 25 μM, and different volumes were automatically injected across the half-area 96-well plate to reach the final volume of 100 μL in each well. Thus, the concentration of rmMBP ranged from 0.5 to 22.5 μM, or from 1:0.1 to 1:4.5 [actin]:[rmMBP] molar ratio. The plate was shaken for 30 s, and the emission intensity was measured for 30 min at 27 °C. Since maximal fluorescence intensity was always observed after 5 min, this time point was used for the comparison of all titration curves. In the experiments where the effect of DPC on MBP-induced actin polymerization was studied, stocks of rmC1, rmC8, rmΔC, and rmΔN were prepared at a concentration of 25 μM in the G buffer, supplemented with 20 mM DPC.

Actin Bundling and Actin−rmMBP Binding. To test the bundling and binding of rmMBPs with G- or F-actin, varying concentrations of rmC1, rmC8, rmΔC, or rmΔN (from 0.5 to 22.5 μM) were added to 5 μM G- or F-actin in a total volume of 100 μL, in the presence or absence of 20 mM DPC. In the experiments in which F-actin was used, G-actin was first polymerized into F-actin by addition of KCl to a final concentration of 50 mM, along with 1 mM EGTA and 2 mM $MgCl_2$. The samples were incubated at room temperature for 30 min, followed by centrifugation at 18000g for 2 h. Under these conditions, only rmMBP bound to highly bundled actin precipitated, but free rmMBP or unbundled actin stayed in the supernatant. The supernatants were transferred to separate tubes, and 80 μL was mixed with 20 μL of 5× sample buffer (60 mM Tris-HCl, pH 6.8, 25% glycerol, 2% SDS, 14.4 mM β-mercaptoethanol, and 0.1% bromophenol blue). The pellets were resuspended in 25 μL of 5× sample buffer and topped up with water to a final volume of 125 μL. Samples (30 μL) from both pellets and supernatants were analyzed for the presence of rmMBP and actin by 14% discontinuous SDS−PAGE (*35*). Following the electrophoresis, gels were stained for 2 h (10% (v/v) acetic acid, 45% (v/v) methanol, and 0.1% (w/v) Coomassie Blue R-250) and destained (10% (v/v) acetic acid and 10% (v/v) methanol) overnight. The bands corresponding to actin monomers or to rmMBP, and sections from the clear part of the same gel (to remove the effect of the background), were excised using a homemade cutting device (8 × 10 mm^2). The stain was extracted from bands (and clear sections) using 1 mL of the extraction solution (3% (w/v) SDS, 50% (v/v) 2-propanol) per band, and the absorbance was measured at 595 nm (*38*). The amount of rmC1, rmC8, rmΔC, rmΔN, and actin in the bands was calculated on the basis of a standard curve obtained by loading known amounts of the above proteins on the same gel. To present actin bundling, we plotted the percentage of bundled actin (fraction of actin determined in the pellet out of the total amount added to the reaction mixture) vs the molar ratio of rmMBP/actin in the reaction. To analyze the binding of rmMBP to actin, the fractional saturation of actin ($[MBP]_{bound}/[actin]_{total}$) was plotted vs the total rmMBP concentration ($[MBP]_{total}$), and the dissociation constants (K_d) were obtained using nonlinear curve fitting with weighted regression to a quadratic equation (Origin Pro 8; OriginLab Corp., Northampton, MA):

$$[MBP]_{bound}/[actin]_{total} = (([MBP]_{total} + n[actin]_{total} + K_d) - (([MBP]_{total} + n[actin]_{total} + K_d)^2 - 4n[MBP]_{total}[actin]_{total})^{0.5})/2[actin]_{total} \quad (1)$$

where $[MBP]_{total}$ is the concentration of rmC1, rmC8, rmΔC, or rmΔN added to the reaction, $[actin]_{total}$ is the total actin concentration, and n is the number of rmMBP molecules bound to an actin molecule (*39*).

Phosphorus Assay. To test the amount of DPC bound to each of the rmMBP variants upon interaction with actin, two different concentrations of rmC1, rmC8, rmΔC, or rmΔN (from 5 and 22.5 μM) were added to 5 μM G-actin in a total volume of 100 μL, in the presence of 20 mM DPC. The samples were incubated at room temperature for 30 min, followed by centrifugation at 18000g for 2 h. Since the only source of phosphorus was from DPC, the pellets were resuspended in 100 μL of 0.4% SDS and subjected to phosphorus detection using Micro-Bartlett phosphorus assay (*40*).

Transmission Electron Microscopy (*TEM*). Transmission electron microscopy was used to examine the morphology of the rmMBP−actin assemblies. Samples were prepared as previously described (*41*). Briefly, each rmMBP variant was allowed to interact with G-actin at a 4.5 to 1 molar ratio (rmMBP variant to actin) in the G buffer. The samples were negatively stained with uranyl acetate, air-dried, and examined using a Philips CM10 transmission electron microscope.

Solid-State NMR Spectroscopy. For all samples to be studied by solid-state NMR spectroscopy, G-actin was first polymerized into F-actin using 50 mM KCl, 1 mM EGTA, and 2 mM $MgCl_2$. Freeze-dried uniformly ^{13}C,^{15}N-labeled rmMBP variants were dissolved in G buffer containing 50 mM KCl, 1 mM EGTA, and 2 mM $MgCl_2$. When needed, rmMBP samples were mixed with DPC to a final DPC concentration of 20 mM and incubated for 30 min at 42 °C. Both protein solutions were then mixed at a 2 to 1 rmMBP to actin molar ratio, incubated at room temperature for 1 h, and then centrifuged at 18000g for 90 min to collect the rmMBP−actin bundles. The pellets were then center-packed in a regular 3.2 mm magic-angle spinning rotor for NMR measurements. Eight different samples were prepared according to this method using four different forms of rmMBP: the rmC1 and rmC8 charge components and the N-terminal deletion (rmΔN) and C-terminal deletion (rmΔC) variants. In four of the samples, unbound rmMBP interacted with F-actin, whereas in the other four samples, DPC-bound rmMBP interacted with F-actin.

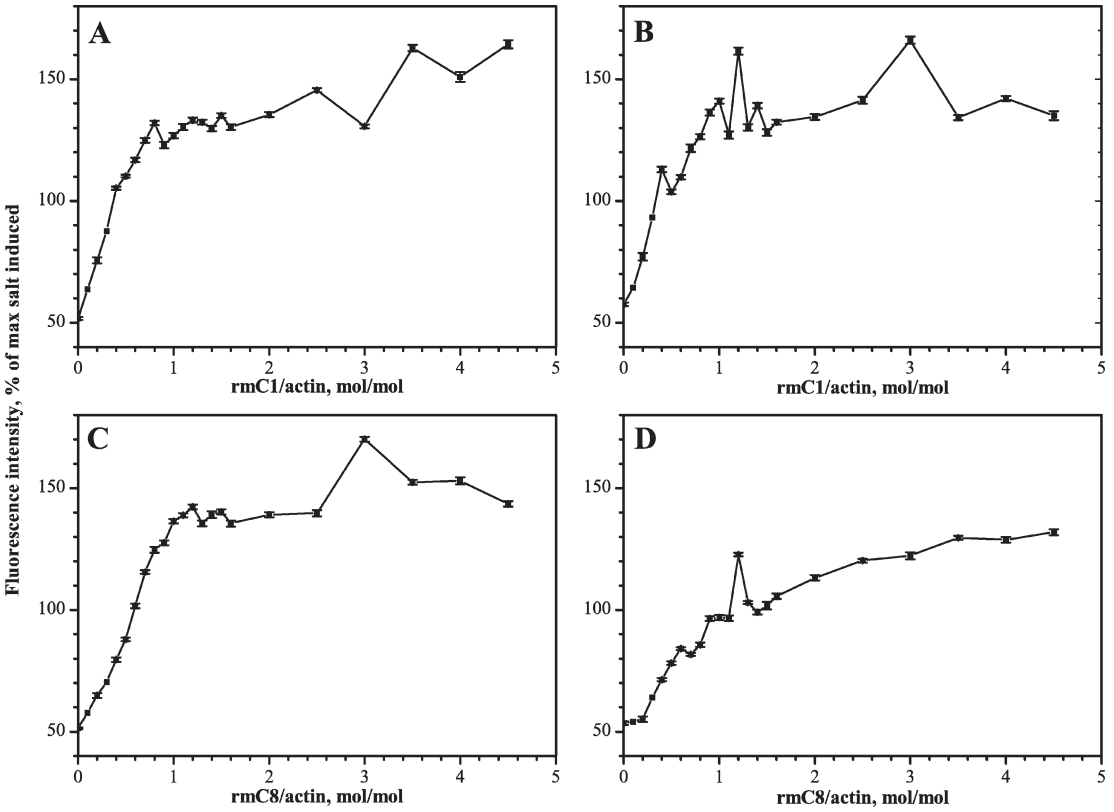

FIGURE 2: Dependence of fluorescence enhancement caused by actin polymerization on the molar ratio of rmMBP variant to actin. All reactions were carried out in G buffer at 27 °C and contained 5 μM G-actin with various concentrations of rmMBP variant in the presence or absence of DPC micelles. (A) Actin polymerization caused by rmC1 alone. (B) Actin polymerization caused by rmC1 in the presence of DPC micelles. (C) Actin polymerization caused by rmC8 alone. (D) Actin polymerization caused by rmC8 in the presence of DPC micelles. Shown in each panel is a representative result out of three independent experiments. The data points in the representative experiment are presented as mean ± standard deviation of three readings of the same sample. Data points are expressed as a percentage of the maximal fluorescence intensity observed in the control experiment in which actin polymerization was induced by F buffer (50 mM KCl, 1 mM EGTA, and 2 mM $MgCl_2$) alone. Note: In the control experiments with DPC alone at concentrations in the range of 1−20 mM, no actin polymerization was observed.

All samples were prepared at the same molar ratio but with a varying final rmMBP content in the NMR sample.

All NMR measurements were performed on a Bruker Avance III spectrometer (Bruker BioSpin, Germany), operating at 600.130 MHz proton frequency and equipped with a Bruker triple-resonance $^{1}H-^{13}C-^{15}N$ 3.2 mm E-Free magic-angle spinning probe (*41*). We collected one-dimensional ^{13}C cross-polarization (CP) and two-dimensional $^{13}C-^{13}C$ dipolar-assisted rotational resonance (DARR) correlation spectra for all eight samples at two different temperatures, namely, +2 and −13 °C, and at a spinning frequency of 12 kHz.

RESULTS

Actin Polymerization Effected by rmC1, rmC8, rmΔC, and rmΔN. In addition to the most-studied function of MBP, which is to maintain the structural stability of the myelin sheath by adhesion of the cytoplasmic leaflets of the oligodendrocyte membrane (*42*−*45*), it is also known that MBP in solution causes polymerization of G-actin to F-actin and bundling of the microfilaments (*8*, *16*−*18*, *46*−*48*). However, the mechanism of interaction, and the potentially different roles of the various interacting domains of MBP when membrane-associated, remains unclear. In this paper, we present a detailed comparison of the interaction of actin with two different charge components and with two different MBP segments, in the presence or absence of DPC, used to mimic the natural lipidic environment of the protein. Although DPC is a zwitterionic lysolipid, it is expected to interact with specific segments of MBP and induce local, ordered secondary structure (*22*, *31*). Although the extent of insertion of the basic protein into the phospholipid membrane depends on its composition and lateral pressure (*49*, *50*), the use of a nonaggregating, monolayer system such as DPC micelles allows the use of solution fluorescence techniques to measure actin polymerization. Vesicles comprising negatively charged lipids will be aggregated by any of the rmMBP variants used (*27*, *51*), necessitating the use here of lysolipid micelles which do not aggregate. For this present study, we have used the full-length, unmodified recombinant murine 18.5 kDa MBP (rmC1), its pseudodeiminated form (rmC8), and two deletion variants, rmΔC and rmΔN (Figure 1) for C- and N-terminal deletions of rmC1, respectively (*32*, *33*).

The increase in the fluorescence intensity of the pyrene-labeled actin was first used as a measure of actin polymerization caused by rmMBP. In this series of experiments, salt-induced polymerization served as a control for the quality of the actin preparation, and its achieved maximal fluorescence intensity was set to 100% for the purpose of normalization. Data for all four rmMBP variants are presented in Figures 2 (charge variants) and 3 (deletion variants). Each pair will be discussed in turn.

We first followed the rate of G-actin polymerization induced by different concentrations of rmC1 and rmC8 (data not shown) and found that the maximal fluorescence intensity was always observed after about 5 min. As shown in Figure 2, increasing concentrations of rmC1 (Figure 2A,B) and rmC8 (Figure 2C,D) caused an enhancement in fluorescence intensity, with the titration

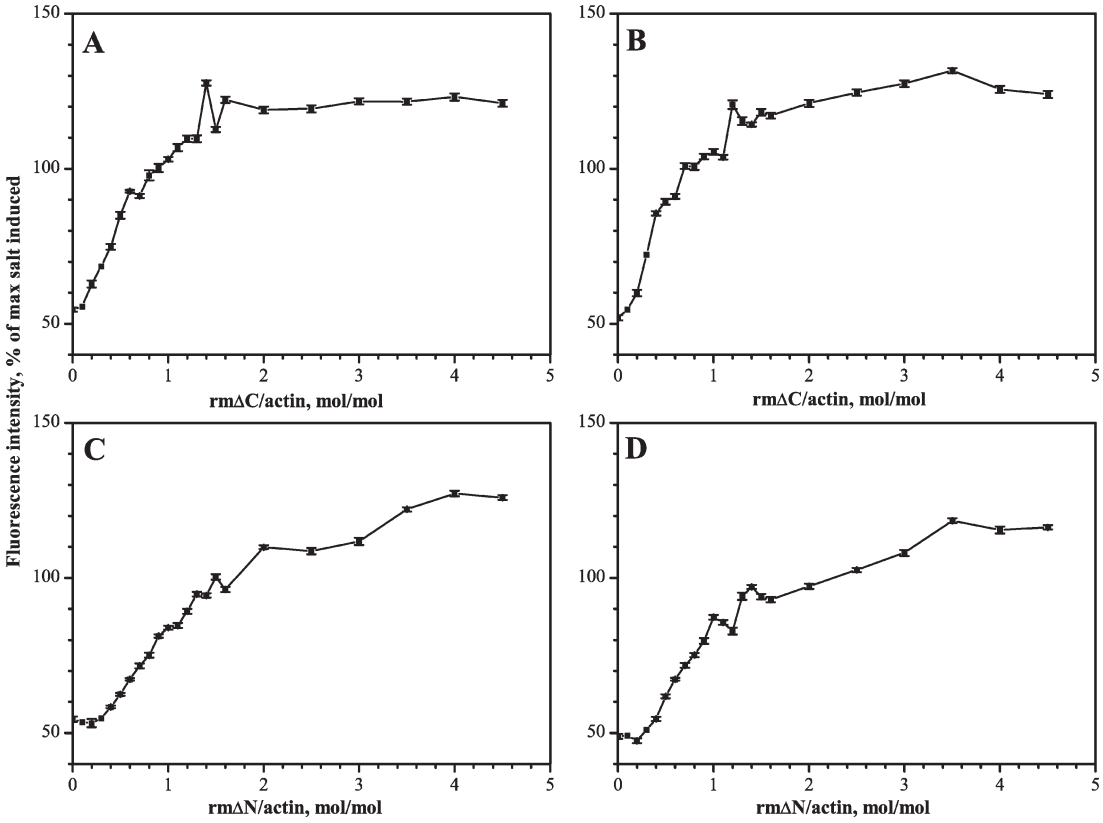

FIGURE 3: Dependence of fluorescence enhancement caused by actin polymerization on the molar ratio of rmMBP truncated variant to actin. All reactions were carried out in G buffer at 27 °C and contained 5 μM G-actin with various concentrations of the rmMBP variant in the presence or absence of DPC micelles. (A) Actin polymerization caused by rmΔC alone. (B) Actin polymerization caused by rmΔC in the presence of DPC micelles. (C) Actin polymerization caused by rmΔN alone. (D) Actin polymerization caused by rmΔN in the presence of DPC micelles. Shown in each panel is a representative (out of three independent experiments) result (mean ± standard deviation of three readings of the same sample), where data points are expressed as a percentage of the maximal fluorescence intensity observed in the control experiment in which actin polymerization was induced by F buffer alone. Note: In the control experiments with DPC alone at concentrations in the range of 1−20 mM, no actin polymerization was observed.

curve having a sigmoidal shape. Both isoforms caused the same fluorescence intensity level at a saturation point that was recorded at a molar ratio of rmMBP to actin of ~0.5 for the rmC1 component and closer to 1 for the rmC8 component. However, at all given concentrations of full-length rmMBP, the initial rate of actin polymerization was faster in the case of rmC1 (data not shown), and at low molar ratios, rmC1 was more active than rmC8 (Figure 2).

It has previously been demonstrated that electrostatic attraction was the major factor affecting the association of MBP with actin (*17*, *18*) and that MBP could bind actin filaments to the surface of negatively charged lipid vesicles (*16*, *17*), suggesting the protein's potential to anchor actin to the oligodendrocyte membrane *in vivo*. In this study, we used DPC, a lysolipid with a net neutral charge and a critical micelle concentration of 1 mM, as a membrane-mimic. (As previously indicated, MBP interacts with and aggregates phospholipid vesicles, thus precluding any solution spectroscopic approach.) In the presence of DPC, the differences between rmC1 and rmC8 in their ability to polymerize G-actin became more obvious. Particularly, to reach the maximal fluorescence intensity level required ~3 times more rmC8 than rmC1 in the presence of DPC (Figure 2), and the maximal level was lower in the case of rmC8 (Figure 4). Since no major differences were observed for actin polymerization by rmC1 in the absence or presence of DPC, this result suggests that the actin-interacting domains in the MBP polypeptide chain are available even in a lipidic environment and confirms that the interaction

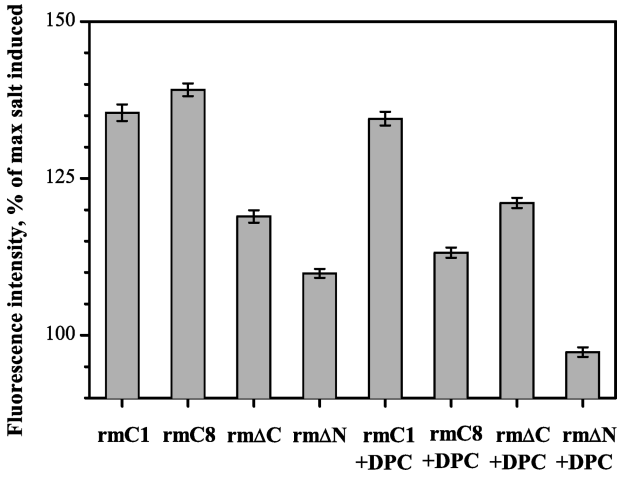

FIGURE 4: Polymerization of G-actin by different forms of rmMBP (full-length charge components rmC1 and rmC8, deletion variants rmΔC and rmΔN). All reactions contained 5 μM G-actin in G buffer, and polymerization was induced by different variants of rmMBP at a molar ratio of 1 to 2 (actin to rmMBP). The results are presented as an average value for triplicate samples ± standard deviation.

between MBP and actin can occur when MBP is bound to the oligodendrocyte membrane.

Thus, in our next set of experiments we tried to identify those interaction domains in MBP more precisely. It was previously shown by others that peptides derived from preparations of 18.5 kDa

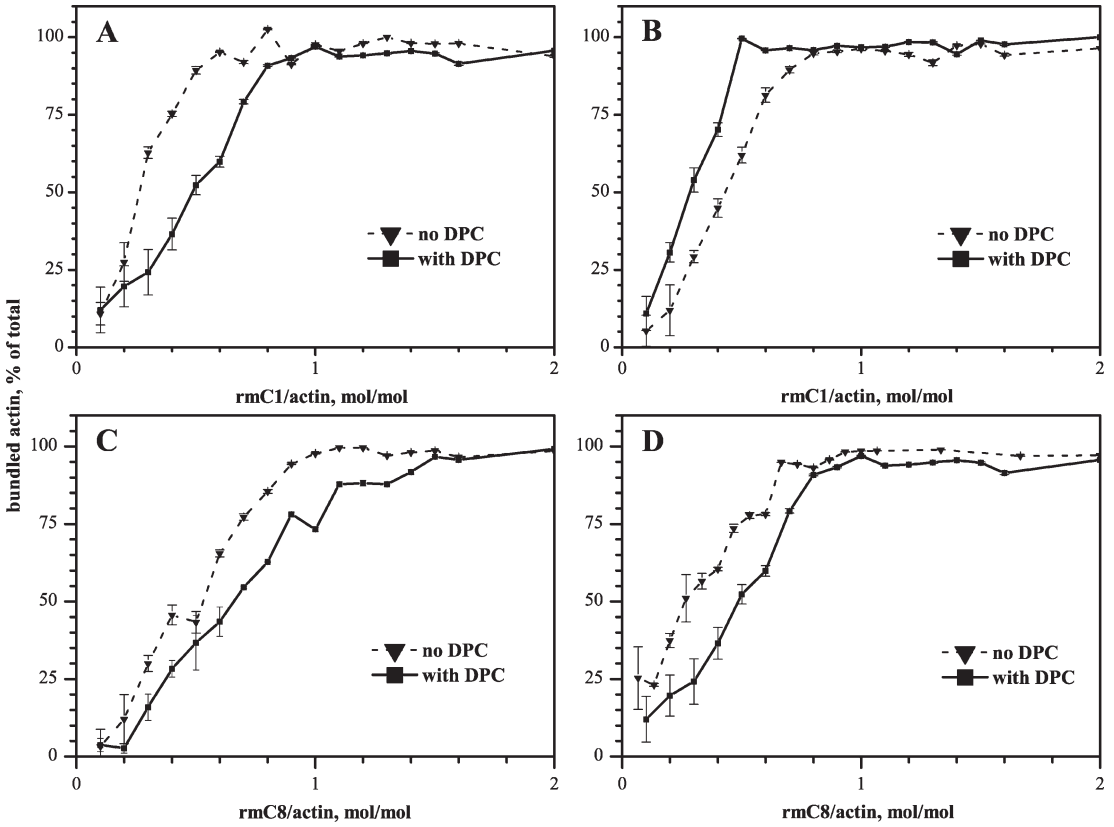

FIGURE 5: Effects of DPC micelles on the bundling of actin by the rmC1 and rmC8 charge variants of rmMBP. All reactions were carried out in G buffer at 27 °C and contained either 5 μM G-actin or preformed F-actin (polymerized by salt), with subsequent addition of various concentrations of rmMBP charge variants in the presence or absence of DPC. Following a 30 min incubation, bundled actin was pelleted by centrifugation at 18000*g* for 30 min. Pellet and supernatant were subjected to SDS−PAGE analysis for actin detection (for details see Materials and Methods). The total amount of actin added to the reactions was set as 100%. (A) G-Actin polymerization and bundling caused by rmC1. (B) F-Actin bundling caused by rmC1. (C) G-Actin polymerization and bundling caused by rmC8. (D) F-Actin bundling caused by rmC8. Note: In the control experiments with DPC alone at concentrations in the range of 1−20 mM, no actin bundling was observed.

MBP purified from brain, specifically the 1−43 and 96−168 segments, exhibited a very strong actin-polymerization activity (*48*). Therefore, here, we used two recombinant deletion variants of rmC1, one comprising the N-terminal two-thirds of the sequence (A1-G105W-His_6) and another missing the N-terminal one-third of the sequence (M0-D57-R168-Leu-Glu-His_6). These proteins are referred to as rmΔC and rmΔN, respectively. The results presented in Figure 3 show that both deletion variants were able to cause actin polymerization, although rmΔN caused less overall polymerization at lower molar ratios of rmMBP to actin. The maximal level of polymerization was observed at a molar ratio of 1.5 in the case of the rmΔC variant and at higher than 2 for the rmΔN protein. At a molar ratio of 2 where actin polymerization was maximal, both deletion variants yielded an overall lower degree of polymerization than rmC1 (Figure 4), with rmΔC being slightly higher than rmΔN, suggesting that the interaction domains are located along the whole 18.5 kDa MBP sequence. This result agrees with our previous study where, using magic-angle spinning solid-state NMR spectroscopy, we showed that the potential interacting fragments can be scattered along the whole rmC1 sequence and can undergo ordered secondary structure changes upon interaction with actin (*41*). However, the comparison of the polymerizing activity of the deletion variants at the same rmMBP/actin molar ratio of 2 in the presence of DPC shows a reduction in the activity of the rmΔN variant, whereas rmΔC exhibited the same activity (Figure 4), signifying the more important role of the N-terminal part of lipid-associated MBP in the polymerization of G-actin.

Actin Microfilament Bundling Effected by rmC1, rmC8, rmΔC, and rmΔN. MBP has also been shown to assemble filamentous actin (F-actin) into bundles *in vitro* (*8*, *17*, *18*, *46*, *47*). In this study, using a sedimentation assay followed by polyacrylamide gel electrophoretic analysis, we compared the ability of rmC1, rmC8, rmΔN, and rmΔC to bundle F-actin in the presence and absence of DPC. (Unbundled F-actin cannot be pelleted at low centrifugation speed, and DPC alone had no effect whatsoever.) We used both G-actin and preformed F-actin (salt-polymerized) as starting material to compare the bundling ability of the different rmMBP variants. It was observed that, in the presence of DPC, more rmMBP was required to bundle actin when it was added to G-actin than to F-actin (compare Figure 5, panels A and C, with Figure 5, panels B and D, respectively), because two separate processes were involved, first polymerization and then bundling. Although rmC1 appeared to be more active than rmC8, when we used G-actin as the starting material, both variants exhibited a similar bundling activity in the case of F-actin, and both were capable of bundling 100% of the actin available. In the experiment where rmMBP was added to G-actin in the absence of DPC, the maximal bundling was observed at an rmMBP to actin ratio of ~0.6 for rmC1 and 1 for rmC8.

When actin was initially polymerized with salt and then bundled by adding rmMBP in the absence of DPC, the maximal bundling level was achieved at rmMBP/actin ratios of ~0.7 and 0.8 for rmC1 and rmC8, respectively. Moreover, in the presence of DPC, the ability of rmC1 to bundle actin starting from G-actin was significantly decreased but appeared to be slightly higher when

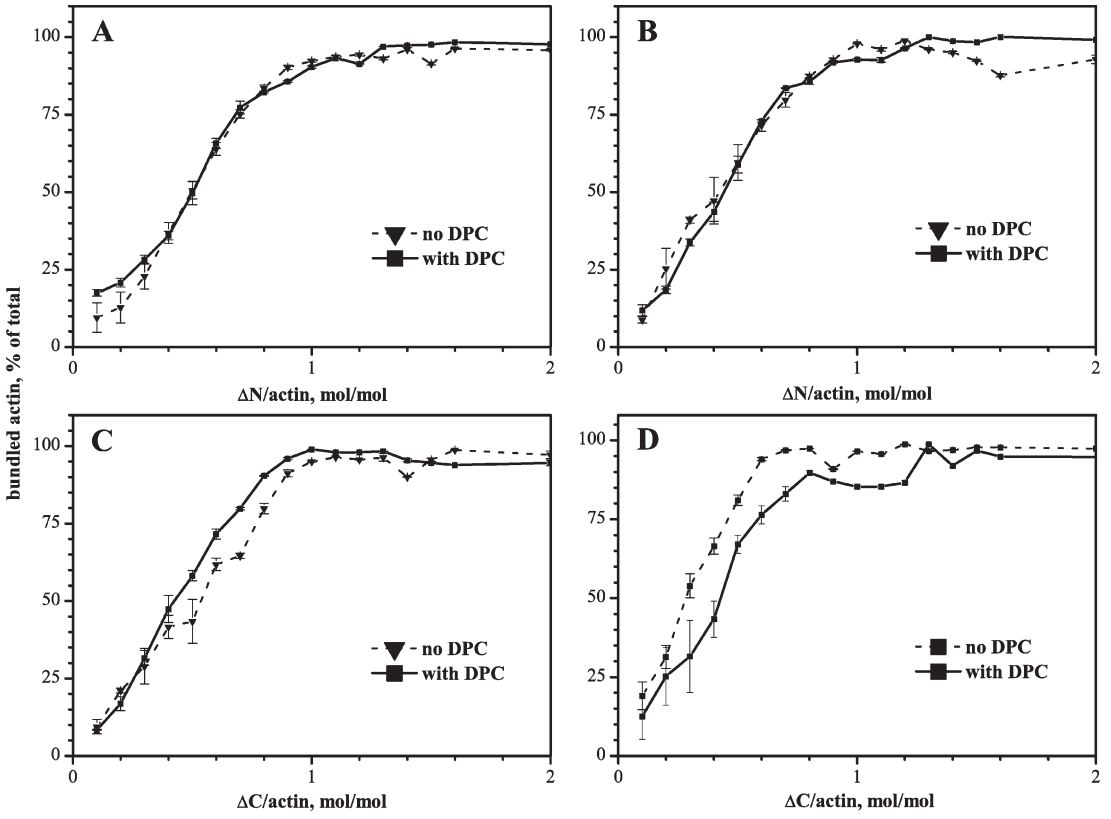

FIGURE 6: Effects of DPC micelles on the bundling of actin by the rmΔN and rmΔC deletion variants of rmMBP. All reactions were prepared in G buffer at 27 °C and contained 5 μM G-actin or preformed F-actin (polymerized by salt) with various concentrations of rmMBP deletion variants in the presence or absence of DPC micelles. Following a 30 min incubation, bundled actin was pelleted by centrifugation at 18000*g* for 30 min. Pellet and supernatant were subjected to SDS−PAGE analysis for actin detection (for details see Materials and Methods). The total amount of actin added to the reactions was set as 100%. (A) G-Actin polymerization and bundling caused by rmΔN. (B) F-Actin bundling caused by rmΔN. (C) G-Actin polymerization and bundling caused by rmΔC. (D) F-Actin bundling caused by rmΔC. Note: In the control experiments with DPC alone at concentrations in the range of 1−20 mM, no actin bundling was observed.

the starting material was F-actin. In the case of rmC8-induced actin bundling in the presence of DPC, the activity was decreased to a certain extent, regardless of whether the starting material was G- and F-actin. Thus, in contrast to the differences observed in the maximal polymerization ability of rmC1 and rmC8 in the presence of DPC (Figure 4), both charge components bundled 100% of the actin, though a lower concentration of the more cationic rmC1 was required.

In the same way, the bundling ability of the rmMBP deletion variants was assayed (Figure 6). Interestingly, we did not find any effect of DPC on the actin bundling induced by either rmΔC or rmΔN. Although the latter form exhibited slightly decreased activity at low rmMBP/actin ratios, with a more pronounced initial lag phase, both variants bundled 100% of the actin. Therefore, in agreement with the results on actin polymerization caused by the rmMBP deletion variants, bundling of actin also seems to depend on a specific domain in the MBP sequence, particularly the N-terminal domain that has a slightly higher bundling ability at low rmMBP/actin molar ratios (Figure 6A,C).

Additionally, using transmission electron microscopy, we compared the morphology of actin bundles assembled by different rmMBP variants (examples are presented in Figure S1 in the Supporting Information). At all molar ratios, in either the presence or absence of DPC, bundles were observed in the reaction mixtures with all rmMBP variants. Only actin bundled by rmC8 appeared to be slightly different: the bundles were thinner and less compact than others. Also, the presence of DPC micelles did not affect the morphology of actin bundles.

Binding of rmMBP Variants to G- and F-Actin. In the present study, we have revisited the mechanism of MBP binding to G- and F-actin (*8*, *16*−*18*, *41*, *48*) and have investigated the effect of DPC (nonaggregating membrane mimic) on this binding. Using the sedimentation assay described above (an example is presented in Figure S2 in the Supporting Information), we compared and characterized the binding parameters of different rmMBP variants with actin (Table 2). Since it was not possible to detect directly the amount of free (unbound) rmMBP in the binding assay, all of our results are presented as a fractional saturation (see Materials and Methods). According to our experimental design, we used actin as a receptor and each rmMBP variant as a ligand. Since microgram amounts of proteins are required for gel-based analysis of the sedimentation assay, the concentration of actin ("receptor") in the binding experiments was much higher (5 μM) than the anticipated K_d (nanomolar range). Under these conditions, the dissociation constant cannot be detected precisely, but the stoichiometry of binding can be measured accurately. Thus, we present the K_d values obtained from different binding experiments in Table 2, but mostly we compared the binding of the different rmMBP variants to actin qualitatively rather than quantitatively.

Another important question for investigation was to detect if DPC micelles stay bound to rmMBP variants upon interaction with actin. Since the only source of phosphorus in our experiments was DPC, we quantified its amount in the actin−rmMBP complexes obtained following the sedimentation assay using a phosphorus assay (see Materials and Methods section). Surprisingly,

Table 2: Parameters of Binding of rmMBP Variants to Actin[a]

	rmC1				rmC8				rmΔC				rmΔN			
	+DPC		−DPC		+DPC		−DPC		+DPC		−DPC		+DPC		−DPC	
	G	F	G	F	G	F	G	F	G	F	G	F	G	F	G	F
K_d, nM	7.6 ± 2.3	14.3 ± 2.7	66.6 ± 6.8	65.3 ± 9.2	22.4 ± 2.6	95.9 ± 3.8	ND	52.6 ± 4.5	101.2 ± 5.88	276.3 ± 6.0	155.2 ± 13.7	91.7 ± 6.5	25.2 ± 2.4	10.5 ± 1.8	255.2 ± 13.5	93.9 ± 5.7
n	1.32 ± 0.04	0.99 ± 0.02	2.06 ± 0.05	1.56 ± 0.06	1.40 ± 0.04	1.17 ± 0.02	ND	1.46 ± 0.04	1.27 ± 0.04	1.40 ± 0.03	1.92 ± 0.08	1.47 ± 0.05	1.38 ± 0.03	1.32 ± 0.02	1.72 ± 0.08	1.49 ± 0.04

[a]Binding parameters were determined from the experiments presented in Figures 7 and 8. Here, "G" and "F" refer to G-actin and F-actin, respectively, and "ND" means "not determined". Results are presented as value ± standard error based on a nonlinear least-squares fitting algorithm using weighted regression to eq 1.

we found that the DPC/rmMBP (all variants) ratio was ~40 detergent molecules per 1 protein, or 1 micelle per rmMBP variant. This ratio stayed constant with no influence from the initial rmMBP/actin ratios in the reaction mixtures.

The comparison of binding of rmC1 and rmC8 variants to G- and F-actin is shown in Figure 7. In general, both rmC8 and rmC1 bound to actin under all conditions investigated, but the stoichiometry and affinity of the binding were different. In the case of rmC1 binding to actin in the presence of DPC, the stoichiometry of binding decreased, approaching unity, regardless of whether the starting material was G- or F-actin (Figure 7A,B). Additionally, when preformed F-actin (salt-polymerized) was the starting material, it can be seen from the slope and curvature of the curves presented in Figure 7B that the affinity of binding increased in the presence of DPC. However, in the experiment using G-actin as the starting material, the binding of rmC8 could not be assessed in the absence of DPC (Figure 7C), due to continuous adsorption of more and more of the less cationic rmMBP molecules to the actin. That binding process never reached saturation, even at high rmC8/actin molar ratios (up to 4.5). On the other hand, in the presence of DPC, the binding became more specific with the stoichiometry being 1.4 molecules of rmC8 per 1 molecule of actin. One possible explanation for this result could be that, even though rmC8 was shown to polymerize and bundle 100% of actin (Figure 5C), the morphology of those filaments and bundles could be different; e.g., actin filaments could be of different length and packed more loosely, thus providing more binding sites for rmC8 in the absence of micelles. This suggestion comes in agreement with our previous report where, using small angle integrated light scattering, actin bundles induced by rmC1 scattered more light than those induced by rmC8 (*17*). Here, the results of transmission electron microscopy confirmed that even in the presence of DPC micelles, where binding of rmC8 could be assessed, actin bundles appeared to be packed more loosely than ones assembled by rmC1 (compare panels A and B in Figure S1 of the Supporting Information). Moreover, the binding of rmC8 appeared to be very different when actin was first polymerized by salt to form F-actin and then interacted with rmMBP. As can be seen from the results presented in Figure 7D, in the presence of DPC, fewer rmC8 molecules could bind actin, but the binding could be assessed even in the abscnce of DPC.

Earlier studies have suggested that there were two binding domains for actin in the MBP molecule, one located at the amino and another at the carboxy terminus (*48*). Thus, next we assessed the binding of two deletion variants of MBP to G- and F-actin in the presence of DPC (Figure 8). Indeed, both deletion variants bound to actin, and the binding parameters are presented in Table 2. Again, the effect of DPC mostly was exhibited in the decreased stoichiometry of binding and, in the case of the rmΔN variant, also in increased affinity (based on the curvature of curves presented in Figure 8A,B). Of the two deletion variants tested in the membrane-mimetic environment, the binding of rmΔN (lacking the N-terminal region of the MBP sequence) appeared to be more comparable to the binding of the full-length rmC1.

Solid-State NMR Spectroscopy. We have previously studied the association of full-length rmC1 with F-actin (in the absence of lipids) by Fourier transform infrared and magic-angle spinning solid-state NMR spectroscopy, in which we demonstrated induced, ordered secondary structure in both protein partners (*41*). Here, similar solid-state NMR experiments were

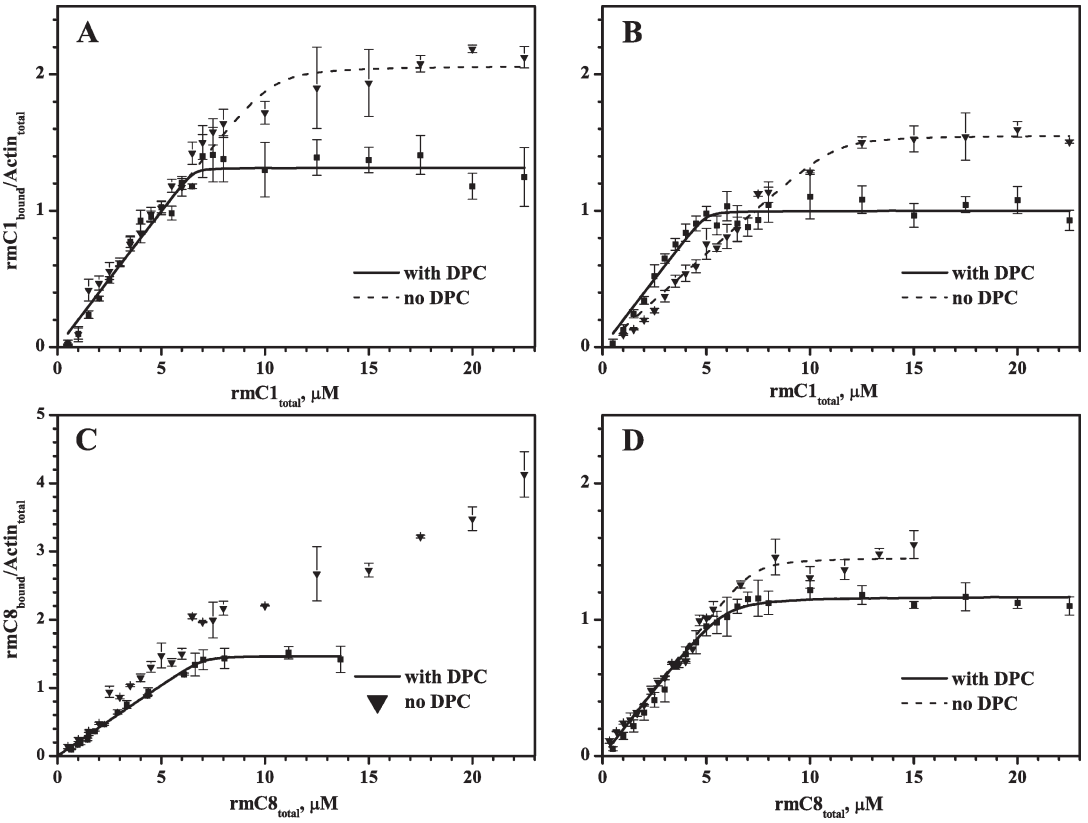

FIGURE 7: Effects of DPC micelles on the binding of actin to rmC1 and rmC8 charge variants. All reactions were prepared in G buffer at 27 °C and contained either 5 μM G-actin or preformed F-actin (polymerized by salt), with subsequent addition of various concentrations of rmMBP charge variant in the presence or absence of DPC micelles. Following a 30 min incubation, bundled actin was pelleted by centrifugation at 18000*g* for 30 min. Pellet and supernatant were subjected to SDS−PAGE analysis for actin and rmMBP detection (for details see Materials and Methods). (A) Binding of rmC1 upon interaction with G-actin. (B) Binding of rmC1 upon interaction with preformed F-actin (salt-polymerized). (C) Binding of rmC8 upon interaction with G-actin. (D) Binding of rmC8 upon interaction with preformed F-actin (salt-polymerized). In all panels, scattered points represent experimentally measured data (mean ± standard deviation of three independent experiments), while solid and dashed lines are the fittings to the experimental data according to eq 1.

carried out on different rmMBP variants in the presence and absence of DPC. In general, the temperature dependence of both one- and two-dimensional spectra of all samples showed similar behavior as in our previously studied system of rmC1−F-actin without lipid (data not shown) (*41*). The signal-to-noise ratio of most of the peaks increased at the expense of line width as the temperature decreased (data not shown). This behavior was attributed to the existence of more than one structural state of rmMBP at lower temperature, due to the polymorphic nature of the interaction between rmMBP and actin (*41*).

Moreover, the resonance dispersion in two-dimensional spectra (Figure 9) showed a similar trend as the lipid-free rmC1−F-actin system studied before, indicating that all different rmMBP variants underwent similar, induced secondary structure changes as was reported earlier (*41*, *51*). For example, Figure 9 shows two $^{13}C-^{13}C$ correlation spectra for two of the samples under consideration: DPC-bound rmC1 and DPC-bound rmΔC with F-actin. In Figure 9A, the resolved fingerprints of some amino acids, namely, Thr and Ala, are identical to those reported earlier for lipid-free rmC1−F-actin (*41*). In addition, the reduced resolution of most of the correlation spectra is a common observation in both DPC−rmC1−F-actin and lipid-free rmC1−F-actin assemblies. This observation indicates that the prior interaction of DPC with rmC1, even though it changed the binding affinity and stoichiometry of the interaction with actin, did not affect the sample homogeneity at the atomic scale. On the other hand, DPC−rmΔC−F-actin (Figure 9B) displayed less crowded correlations attributed both to the lower signal-to-noise ratio, as a result of the reduced protein amount in this sample (~2 mg) compared to that of Figure 9A (~5 mg), and to the smaller protein size in the case of rmΔC (almost two-thirds of rmC1). However, this sample also displayed the same polymorphic behavior as the full-length rmC1 samples.

DISCUSSION

The 18.5 kDa MBP splice isoform has been thought to be primarily a molecular adhesive in CNS myelin, adhering the apposing cytosolic surfaces of the oligodendrocyte membrane to each other (*3*, *4*, *14*). As recently reviewed, in addition to this main function, MBP has been shown to interact with a wide variety of biological ligands including cytoskeletal proteins, calmodulin, SH3-domain containing proteins, and divalent metal cations (*14*, *51*, *51*−*53*). It has been shown in previous studies that two charge components of the "classic" 18.5 kDa MBP, the most cationic (C1) and the least cationic one (C8), were able to polymerize, bundle, and link actin to the phospholipid membranes (*8*, *15*−*17*, *46*−*48*). The polymerization of actin was reversible in the presence of calmodulin (*8*, *17*). In the present study, we have compared the interaction of recombinant murine MBP charge components (rmC1 and rmC8) with G- and F-actin in a membrane-mimetic environment and characterized the binding properties of the N- and C-terminal domains in the MBP sequence.

The results of this investigation confirmed that lipid-associated MBP is able to polymerize G-actin and bundle F-actin. Of two

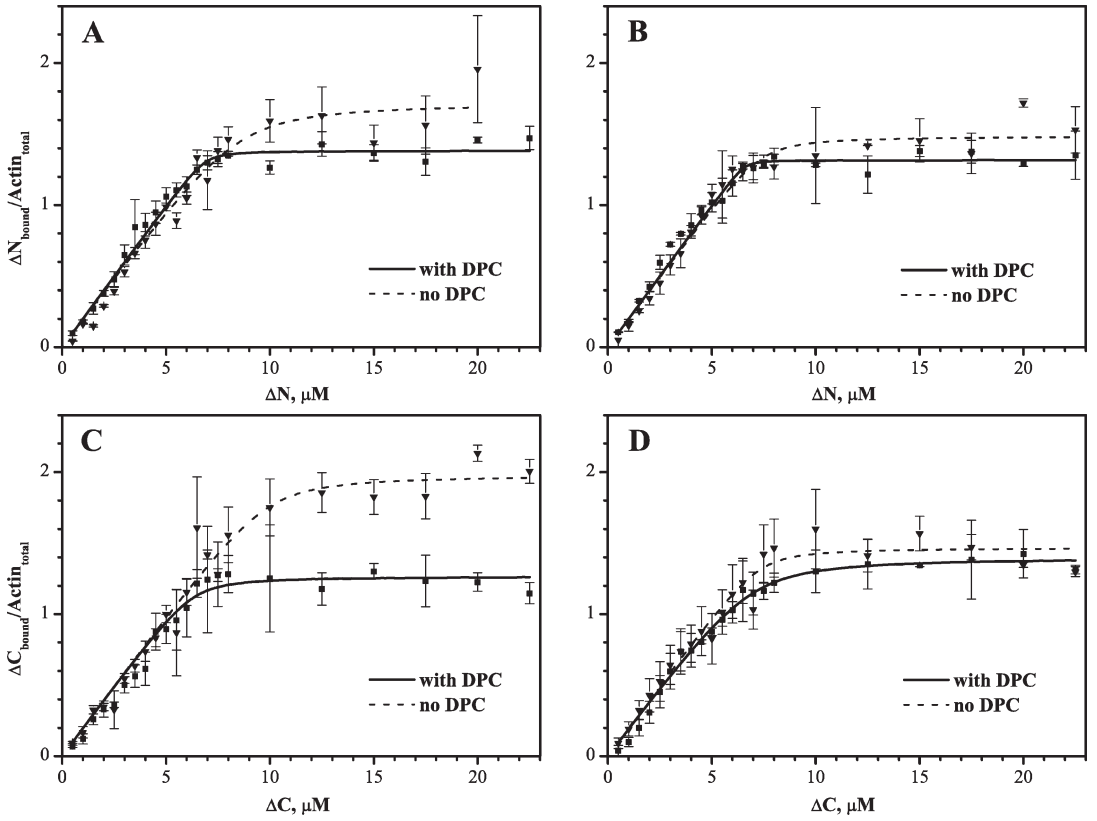

FIGURE 8: Effects of DPC micelles on the binding of actin to rmΔC and rmΔN deletion variants. All reactions were prepared in G buffer at 27 °C and contained 5 μM G-actin or preformed F-actin (polymerized by salt) with various concentrations of rmMBP deletion variant in the presence or absence of DPC micelles. Following a 30 min incubation, bundled actin was pelleted by centrifugation at 18000*g* for 30 min. Pellet and supernatant were subjected to SDS−PAGE analysis for actin and rmMBP detection (for details see Materials and Methods). (A) Binding of rmΔN upon interaction with G-actin. (B) Binding of rmΔN upon interaction with preformed F-actin. (C) Binding of rmΔC upon interaction with G-actin. (D) Binding of rmΔC upon interaction with preformed F-actin. In all panels, scattered points represent experimentally measured data (mean ± standard deviation of three independent experiments), while solid and dashed lines are the fittings to the experimental data according to eq 1.

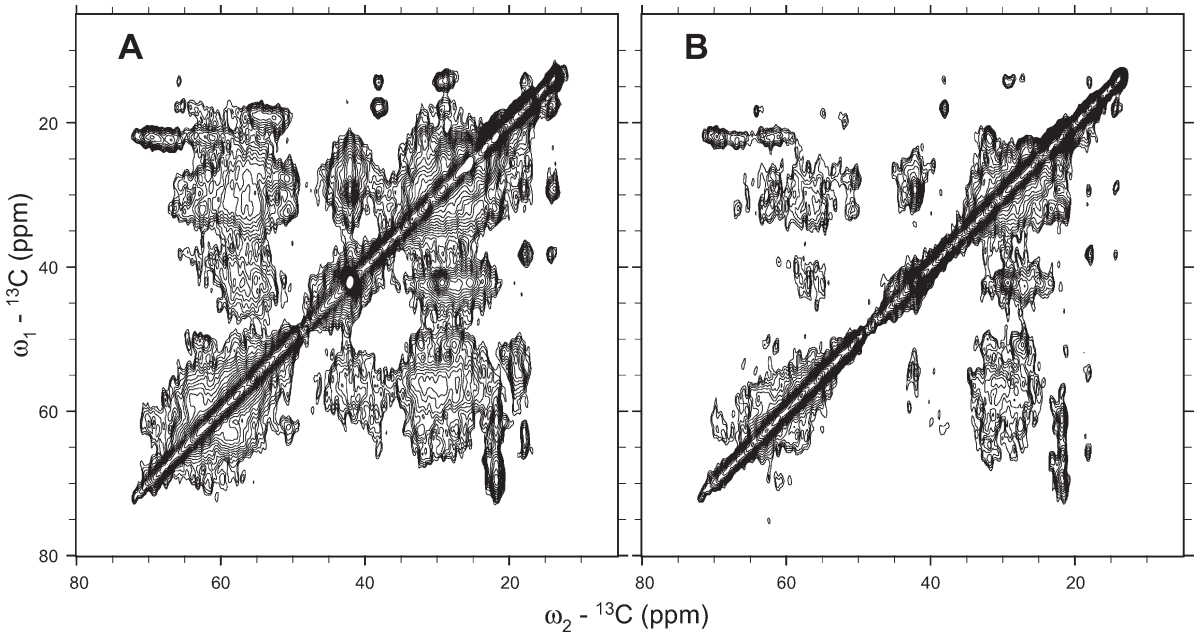

FIGURE 9: Solid-state magic-angle spinning NMR spectroscopy of assemblies of actin with DPC−rmMBP (two variants). Aliphatic regions of two-dimensional DARR (dipolar-assisted rotational resonance) $^{13}C-^{13}C$ correlation spectra of uniformly $^{13}C,^{15}N$-labeled rmMBP in the DPC−rmMBP−actin complex. (A) DPC−rmC1−F-actin. (B) DPC−rmΔC−F-actin. In all experiments, the indirect and direct acquisition times were 4 and 14 ms, respectively, and were apodized with a $\pi/2$-shifted sine-squared window function prior to Fourier transformation. The first contour is cut at 5 times the noise floor, and each following contour level is multiplied by 1.15. Both spectra were collected at $T = -13$ °C, at 12 kHz magic-angle spinning rate, and using a DARR mixing time of 50 ms. The spectra were acquired with 224 and 152 scans per t_1 point for the samples in panels A and B, respectively.

charge components, rmC1 and rmC8, the more cationic protein appeared to be more active at lower molar ratios of rmMBP variant to actin, which is in agreement with our previous findings (*17*). Since a natural lipidic environment is more physiologically relevant to MBP, which, even when membrane-associated, is still significantly mobile and able to interact with other proteins (*26*), the novel approach here was to use the membrane-mimicking conditions (presence of DPC micelles) to compare the actin-assembling capabilities of rmC1 and rmC8. (We review elsewhere the challenges associated with creating an experimentally tractable, myelin-mimetic environment, for MBP (*27*, *28*, *51*).) The use of DPC as a membrane-mimicking environment is common, and in previous studies it has been reported that the stoichiometry of the MBP interaction with DPC was 200 molecules of lipid per 1 protein molecule (*22*, *31*). Since the average number of DPC molecules per micelle ranges from 40 to 60, each MBP can thus bind around four DPC micelles. In contrast, in the present study, we found that upon interaction of different rmMBP variants with actin only one DPC micelle stays bound to MBP in the complex with actin.

In the presence of DPC, the polymerization ability of the less cationic rmC8 was found to be significantly lower than that of the highly positively charged rmC1 protein (*17*). One possible explanation could be that the interaction with DPC micelles masks some positively charged residues in the MBP sequence, and since the charge of rmC8 had already been reduced by +6, this additional masking resulted in decreased polymerization activity. In fact, it has previously been shown that several domains in the polypeptide chain of MBP are capable of penetrating into the hydrophobic core of the DPC micelles (*22*, *24*, *31*). Our previous magic-angle spinning solid-state NMR study of the interaction of rmC1 with actin in an aqueous environment showed that both MBP and actin had mutually induced ordered secondary structure (*41*). The potential sites that might experience changes in the secondary structure in MBP were distributed over the entire sequence, thus suggesting that the entire molecule might be involved in the association with actin.

Here, by studying the ability of two rmMBP deletion variants to polymerize and bundle actin, we further confirmed that the entire sequence of 18.5 kDa MBP is involved in the interaction. Our results showed that though the polymerizing ability of the deletion variants was reduced compared to the full-length rmC1 isoform, they both were able to bundle 100% of the actin. The rmΔN variant, the one lacking 56 amino acids at the amino terminus of the sequence, exhibited lower polymerization and bundling activity than the rmΔC form, which lacked 63 residues at the carboxy-terminal end. The difference in actin-assembling ability appeared to be even more pronounced in the presence of DPC. Although it seems that the N-terminal part of 18.5 kDa MBP is more important for its interaction with actin, the interaction of the C-terminal part of the protein might be physiologically more relevant, because this is the primary binding domain for calmodulin (*28*, *52*). Calmodulin in solution has been shown to cause depolymerization of the MBP-polymerized actin with greater efficiency in the case of rmC8 (*16*, *17*, *47*). This idea is supported here by the results of binding experiments of the two deletion variants of rmMBP to G- and F-actin, particularly in the presence of DPC micelles. We have shown that both variants bound actin during polymerization and/or bundling. In the presence of micelles, the binding was more specific (lower rmMBP/actin ratio), and the affinity was greater for the rmΔN construct (the dissociation constants were 10.5 ± 1.8 nM and 276.3 ± 6.0 nM for rmΔN and rmΔC, respectively). Although the absolute values of K_d could not be used for precise analysis, it can be seen that the curvature of curves presented in Figure 8B,D is different, thus suggesting a greater affinity in the case of rmΔN. Additionally, it is known that the N-terminal part of MBP provides one of the interaction sites with DPC micelles (*31*), thus potentially decreasing its ability to bind actin. Therefore, in the context of MBP's physiological environment, the N-terminal two-thirds of the protein (being membrane-associated) can be responsible for actin polymerization/bundling, and the C-terminal part can bind actin and tether it to the oligodendrocyte membrane. Thus, potentially the C-terminal segment of MBP may represent the regulatory domain for the interaction with actin in a lipid environment. This domain also contains the primary calmodulin-binding segment of 18.5 kDa MBP (*28*, *54*).

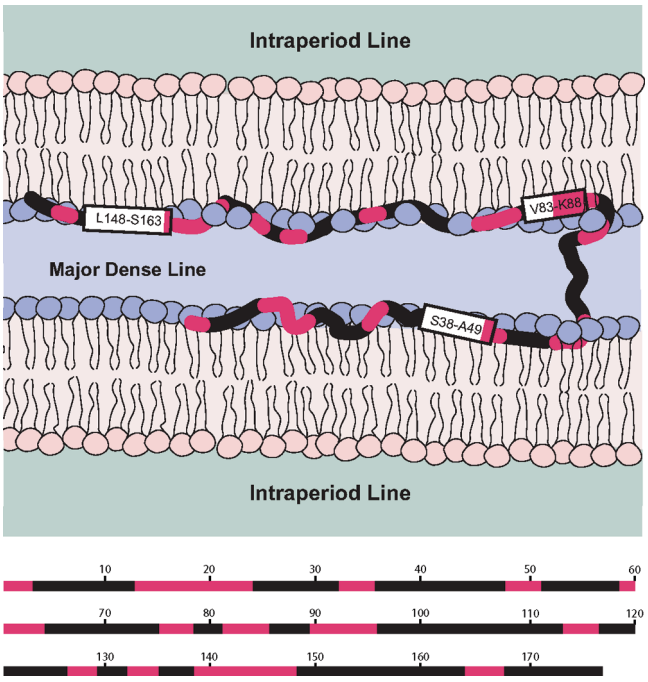

FIGURE 10: Schematic representation of the interaction of MBP with membrane and regions potentially involved in interaction with actin. The details of basic protein−membrane binding are not known, and the arrangement shown in this figure is one out of many possibilities. There is scant evidence for MBP dimerization or oligomerization in myelin, so the protein is presented here as a monomer. The boxes represent the amphipathic α-helices that were proposed based on solution and solid-state NMR spectroscopic studies (*26*, *28*, *52*) and electron paramagnetic resonance investigations (*23*, *55*), including one that focused on the immunodominant epitope (Pro82−Pro93, murine 18.5 kDa sequence numbering) (*23*, *25*). The proline-rich segment immediately following (and slightly overlapping) this epitope forms a transient polyproline type II helix (*10*), and the region comprising Pro120−Arg160 represents a primary binding site for Ca-activated calmodulin (*28*, *51*). In red, we denote the regions of MBP that might undergo changes in secondary structure upon interaction with actin (*41*).

Our solid-state NMR spectroscopy data on DPC-bound rmMBP showed that, although the prior interaction of MBP with DPC improved its binding specificity, MBP−actin interactions are still polymorphic, even in the membrane-mimicking environment of DPC micelles (Figure 9) (*51*).

In the 18.5 kDa splice isoform of MBP, basic residues are distributed along the sequence, and the charge density is fairly uniform (*17*, *18*). These multiple sites allow one MBP molecule to cross-link two or more actin filaments together and arrange them

into bundles. Moreover, some of those basic residues can be involved in the interaction of MBP with the oligodendrocyte membrane, whereas other residues will be available to bind to and anchor actin to the membrane. In Figure 10, we present a model of a proposed arrangement of MBP in the myelin sheath. First, based on information acquired from previous electron paramagnetic resonance and NMR spectroscopic investigations, we know that the N-terminal part of the protein, particularly the S38-A49 region, is embedded in the hydrophobic portion of the bilayer (*26*, *55*). The central region of the protein penetrates the membrane and also associates electrostatically with the phospholipid headgroups (lysine snorkeling), and the C-terminal part penetrates the hydrophobic core of the membrane again (*23*, *26*). In the case of the pseudodeiminated rmC8 component, the net charge reduction results in the dissociation of some sites in the C-terminal part of the protein from the lipid bilayer, making it more accessible for the interaction with different ligands (*55*, *56*). Second, from our previous solid-state NMR structural study of the interaction of lipid-free rmC1 with actin, we posit that the potential regions of MBP involved in the interaction with actin are distributed through the entire molecule, and within the context of the lipid bilayer (oligodendrocyte membrane) some of them remain accessible for the interaction (*26*, *41*). Finally, the C-terminal domain of MBP contains the primary binding site for Ca^{2+}-activated calmodulin (*28*, *54*) and thus could play a crucial role in the regulation of MBP's actin polymerizing activity and its ability to link actin to the membrane.

In conclusion, the results of this study confirm that MBP can act as a linker between actin and membrane and thus participate in the rearrangement (polymerization and bundling) of actin within myelin. There are multiple binding domains located in the MBP sequence which are important for the cross-talk between actin filaments and the oligodendrocyte membrane, which, in turn, can control cell morphology, thereby maintaining functional and healthy myelin assembly in the CNS.

ACKNOWLEDGMENT

We are grateful to Drs. Vladimir Ladizhansky (Guelph), John Dawson (Guelph), and Joan Boggs (Hospital for Sick Children, Toronto) for helpful discussions and comments on the manuscript.

SUPPORTING INFORMATION AVAILABLE

Transmission electron micrographs of the actin filaments bundled by different rmMBP variants (Figure S1) and a representative set of SDS−PAGE gels used for the binding assay (Figure S2). This material is available free of charge via the Internet at http://pubs.acs.org.

REFERENCES

1. Martin, R., McFarland, H. F., and McFarlin, D. E. (1992) Immunological Aspects of Demyelinating Diseases. *Annu. Rev. Immunol. 10*, 153–187.
2. Feng, J. M., Fernandes, A. O., Campagnoni, C. W., Hu, Y. H., and Campagnoni, A. T. (2004) The Golli-Myelin Basic Protein Negatively Regulates Signal Transduction in T Lymphocytes. *J. Neuroimmunol. 152*, 57–66.
3. Omlin, F. X., Webster, H. D., Palkovits, C. G., and Cohen, S. R. (1982) Immunocytochemical Localization of Basic Protein in Major Dense Line Regions of Central and Peripheral Myelin. *J. Cell Biol. 95*, 242–248.
4. Readhead, C., Takasashi, N., Shine, H. D., Saavedra, R., Sidman, R., and Hood, L. (1990) Role of Myelin Basic Protein in the Formation of Central Nervous System Myelin. *Ann. N.Y. Acad. Sci. 605*, 280–285.
5. Radivojac, P., Iakoucheva, L. M., Oldfield, C. J., Obradovic, Z., Uversky, V. N., and Dunker, A. K. (2007) Intrinsic Disorder and Functional Proteomics. *Biophys. J. 92*, 1439–1456.
6. Receveur-Bréchot, V., Bourhis, J. M., Uversky, V. N., Canard, B., and Longhi, S. (2006) Assessing Protein Disorder and Induced Folding. *Proteins 62*, 24–45.
7. Boggs, J. M. (2006) Myelin Basic Protein: A Multifunctional Protein. *Cell. Mol. Life Sci. 63*, 1945–1961.
8. Boggs, J. M., Rangaraj, G., Gao, W., and Heng, Y. M. (2006) Effect of Phosphorylation of Myelin Basic Protein by MAPK on its Interactions with Actin and Actin Binding to a Lipid Membrane *in Vitro*. *Biochemistry 45*, 391–401.
9. Harauz, G., Ishiyama, N., Hill, C. M. D., Bates, I. R., Libich, D. S., and Farès, C. (2004) Myelin Basic Protein—Diverse Conformational States of an Intrinsically Unstructured Protein and its Roles in Myelin Assembly and Multiple Sclerosis. *Micron 35*, 503–542.
10. Polverini, E., Rangaraj, G., Libich, D. S., Boggs, J. M., and Harauz, G. (2008) Binding of the Proline-Rich Segment of Myelin Basic Protein to SH3-Domains—Spectroscopic, Microarray, and Modeling Studies of Ligand Conformation and Effects of Post-Translational Modifications. *Biochemistry 47*, 267–282.
11. Smith, G. S. T., Chen, L., Bamm, V. V., Dutcher, J., and Harauz, G. (2010) The Interaction of Zinc with Membrane-Associated 18.5 kDa Myelin Basic Protein: An Attenuated Total Reflectance-Fourier Transform Infrared Spectroscopic Study. Amino Acids [2010 Feb 19, Epub ahead of print].
12. Kim, J. K., Mastronardi, F. G., Wood, D. D., Lubman, D. M., Zand, R., and Moscarello, M. A. (2003) Multiple Sclerosis: An Important Role for Post-Translational Modifications of Myelin Basic Protein in Pathogenesis. *Mol. Cell. Proteomics 2*, 453–462.
13. DeBruin, L. S., and Harauz, G. (2007) White Matter Rafting—Membrane Microdomains in Myelin. *Neurochem. Res. 32*, 213–228.
14. Harauz, G., Ladizhansky, V., and Boggs, J. M. (2009) Structural Polymorphism and Multifunctionality of Myelin Basic Protein. *Biochemistry 48*, 8094–8104.
15. Boggs, J. M. (2008) Myelin Basic Protein Interactions with Actin and Tubulin *in Vitro*: Binding, Assembly, and Regulation, in Myelin Basic Protein (Boggs, J. M., Ed.) pp 149−167, Nova Science Publishers, New York.
16. Boggs, J. M., and Rangaraj, G. (2000) Interaction of Lipid-Bound Myelin Basic Protein with Actin Filaments and Calmodulin. *Biochemistry 39*, 7799–7806.
17. Boggs, J. M., Rangaraj, G., Hill, C. M., Bates, I. R., Heng, Y. M., and Harauz, G. (2005) Effect of Arginine Loss in Myelin Basic Protein, as Occurs in its Deiminated Charge Isoform, on Mediation of Actin Polymerization and Actin Binding to a Lipid Membrane *in Vitro*. *Biochemistry 44*, 3524–3534.
18. Hill, C. M. D., and Harauz, G. (2005) Charge Effects Modulate Actin Assembly by Classic Myelin Basic Protein Isoforms. *Biochem. Biophys. Res. Commun. 329*, 362–369.
19. Dyer, C. A., Philibotte, T. M., Wolf, M. K., and Billings-Gagliardi, S. (1994) Myelin Basic Protein Mediates Extracellular Signals that Regulate Microtubule Stability in Oligodendrocyte Membrane Sheets. *J. Neurosci. Res. 39*, 97–107.
20. Dyer, C. A., Philibotte, T. M., Billings-Gagliardi, S., and Wolf, M. K. (1995) Cytoskeleton in Myelin-Basic Protein-Deficient Shiverer Oligodendrocytes. *Dev. Neurosci. 17*, 53–62.
21. Dyer, C. A., Philibotte, T., Wolf, M. K., and Billings-Gagliardi, S. (1997) Regulation of Cytoskeleton by Myelin Components: Studies on Shiverer Oligodendrocytes Carrying an *Mbp* Transgene. *Dev. Neurosci. 19*, 395–409.
22. Mendz, G. L., Moore, W. J., Kaplin, I. J., Cornell, B. A., Separovic, F., Miller, D. J., and Brown, L. R. (1988) Characterization of Dodecylphosphocholine/Myelin Basic Protein Complexes. *Biochemistry. 27*, 379–386.
23. Bates, I. R., Feix, J. B., Boggs, J. M., and Harauz, G. (2004) An Immunodominant Epitope of Myelin Basic Protein Is an Amphipathic Alpha-Helix. *J. Biol. Chem. 279*, 5757–5764.
24. Farès, C., Libich, D. S., and Harauz, G. (2006) Solution NMR Structure of an Immunodominant Epitope of Myelin Basic Protein. Conformational Dependence on Environment of an Intrinsically Unstructured Protein. *FEBS J. 273*, 601–614.
25. Musse, A. A., Boggs, J. M., and Harauz, G. (2006) Deimination of Membrane-Bound Myelin Basic Protein in Multiple Sclerosis Exposes an Immunodominant Epitope. *Proc. Natl. Acad. Sci. U.S.A. 103*, 4422–4427.
26. Zhong, L., Bamm, V. V., Ahmed, M. A., Harauz, G., and Ladizhansky, V. (2007) Solid-State NMR Spectroscopy of 18.5 kDa Myelin Basic Protein Reconstituted with Lipid Vesicles: Spectroscopic Characterisation

and Spectral Assignments of Solvent-Exposed Protein Fragments. *Biochim. Biophys. Acta 1768*, 3193–3205.
27. Libich, D. S., and Harauz, G. (2008) Solution NMR and CD Spectroscopy of an Intrinsically Disordered, Peripheral Membrane Protein: Evaluation of Aqueous and Membrane-Mimetic Solvent Conditions for Studying the Conformational Adaptability of the 18.5 kDa Isoform of Myelin Basic Protein (MBP). *Eur. Biophys. J. 37*, 1015–1029.
28. Libich, D. S., and Harauz, G. (2008) Backbone Dynamics of the 18.5 kDa Isoform of Myelin Basic Protein Reveals Transient α-Helices and a Calmodulin-Binding Site. *Biophys. J. 94*, 4847–4866.
29. Harauz, G., Ladizhansky, V. (2008) Structure and Dynamics of the Myelin Basic Protein Family by Solution and Solid-State NMR, in Myelin Basic Protein (Boggs, J. M., Ed.) pp 197−232, Nova Science Publishers, New York.
30. Boggs, J. M., Bates, I. R., Musse, A. A., and Harauz, G. (2008) Interactions of the 18.5 kDa Myelin Basic Protein with Lipid Bilayers: Studies by Electron Paramagnetic Resonance Spectroscopy and Implications for Generation of Autoimmunity in Multiple Sclerosis, in Myelin Basic Protein (Boggs, J. M., Ed.) pp 105−125, Nova Science Publishers, New York.
31. Mendz, G. L., Moore, W. J., Brown, L. R., and Martenson, R. E. (1984) Interaction of Myelin Basic Protein with Micelles of Dodecylphosphocholine. *Biochemistry 23*, 6041–6046.
32. Bates, I. R., Libich, D. S., Wood, D. D., Moscarello, M. A., and Harauz, G. (2002) An Arg/Lys→Gln Mutant of Recombinant Murine Myelin Basic Protein as a Mimic of the Deiminated Form Implicated in Multiple Sclerosis. *Protein Expression Purif. 25*, 330–341.
33. Hill, C. M. D., Haines, J. D., Antler, C. E., Bates, I. R., Libich, D. S., and Harauz, G. (2003) Terminal Deletion Mutants of Myelin Basic Protein: New Insights into Self-Association and Phospholipid Interactions. *Micron 34*, 25–37.
34. Bates, I. R., Matharu, P., Ishiyama, N., Rochon, D., Wood, D. D., Polverini, E., Moscarello, M. A., Viner, N. J., and Harauz, G. (2000) Characterization of a Recombinant Murine 18.5-kDa Myelin Basic Protein. *Protein Expression Purif. 20*, 285–299.
35. Laemmli, U. K. (1970) Cleavage of Structural Proteins during the Assembly of Bacteriophage T4. *Nature 227*, 680–685.
36. Pardee, J. D., and Spudich, J. A. (1982) Purification of Muscle Actin. *Methods Cell Biol. 24*, 271–289.
37. Kouyama, T., and Mihashi, K. (1981) Fluorimetry Study of N-(1-Pyrenyl) Iodoacetamide-Labelled F-Actin. *Eur. J. Biochem. 114*, 33–38.
38. Ball, E. H. (1986) Quantitation of Proteins by Elution of Coomassie Brilliant Blue R from Stained Bands after Sodium Dodecyl Sulfate-Polyacrylamide Gel Electrophoresis. *Anal. Biochem. 155*, 23–27.
39. Bligh, S. W., Haley, T., and Lowe, P. N. (2003) Measurement of Dissociation Constants of Inhibitors Binding to Src SH2 Domain Protein by Non-Covalent Electrospray Ionization Mass Spectrometry. *J. Mol. Recognit. 16*, 139–148.
40. Bartlett, G. (1959) Phosphorus Assay in Column Chromatography. *J. Biol. Chem. 234*, 466–468.
41. Ahmed, M. A., Bamm, V. V., Shi, L., Steiner-Mosonyi, M., Dawson, J. F., Brown, L., Harauz, G., and Ladizhansky, V. (2009) Induced Secondary Structure and Polymorphism in an Intrinsically Disordered Structural Linker of the CNS: Solid-State NMR and FTIR Spectroscopy of Myelin Basic Protein Bound to Actin. *Biophys. J. 96*, 180–191.
42. Napolitano, L., Lebaron, F., and Scaletti, J. (1967) Preservation of Myelin Lamellar Structure in the Absence of Lipid. A Correlated Chemical and Morphological Study. *J. Cell Biol. 34*, 817–826.
43. Moscarello, M. A., Brady, G. W., Fein, D. B., Wood, D. D., and Cruz, T. F. (1986) The Role of Charge Microheterogeneity of Basic Protein in the Formation and Maintenance of the Multilayered Structure of Myelin: A Possible Role in Multiple Sclerosis. *J. Neurosci. Res. 15*, 87–99.
44. Smith, R. (1992) The Basic Protein of CNS Myelin: Its Structure and Ligand Binding. *J. Neurochem. 59*, 1589–1608.
45. Moscarello, M. A. (1997) Myelin Basic Protein, the "Executive" Molecule of the Myelin Membrane, in Cell Biology and Pathology of Myelin: Evolving Biological Concepts and Therapeutic Approaches (Juurlink, B. H. J., Devon, R. M., Doucette, J. R., Nazarali, A. J., Schreyer, D. J., and Verge, V. M. K., Eds.) pp 13−25, Plenum Press, New York.
46. Barylko, B., and Dobrowolski, Z. (1984) Ca^{2+}-Calmodulin-Dependent Regulation of F-Actin-Myelin Basic Protein Interaction. *Eur. J. Cell Biol. 35*, 327–335.
47. Dobrowolski, Z., Osinska, H., Mossakowska, M., and Barylko, B. (1986) Ca^{2+}-Calmodulin-Dependent Polymerization of Actin by Myelin Basic Protein. *Eur. J. Cell Biol. 42*, 17–26.
48. Roth, G. A., Gonzalez, M. D., Monferran, C. G., De Santis, M. L., and Cumar, F. A. (1993) Myelin Basic Protein Domains Involved in the Interaction with Actin. *Neurochem. Int. 23*, 459–465.
49. Rosetti, C. M., Maggio, B., and Oliveira, R. G. (2008) The Self-Organization of Lipids and Proteins of Myelin at the Membrane Interface. Molecular Factors Underlying the Microheterogeneity of Domain Segregation. *Biochim. Biophys. Acta 1778*, 1665–1675.
50. Rosetti, C. M., Maggio, B., and Wilke, N. (2010) Micron-Scale Phase Segregation in Lipid Monolayers Induced by Myelin Basic Protein in the Presence of a Cholesterol Analog. *Biochim. Biophys. Acta 1798*, 498–505.
51. Libich, D. S., Ahmed, M. A. M., Zhong, L., Bamm, V. V., Ladizhansky, V., and Harauz, G. (2010) Fuzzy Complexes of Myelin Basic Protein—NMR Spectroscopic Investigations of a Polymorphic Organizational Linker of the Central Nervous System. *Biochem. Cell Biol. 88*, 143–155 (Special Issue on Protein Folding: Principles and Diseases).
52. Harauz, G., and Libich, D. S. (2009) The Classic Basic Protein of Myelin—Conserved Structural Motifs and the Dynamic Molecular Barcode Involved in Membrane Adhesion and Protein-Protein Interactions. *Curr. Protein Pept. Sci. 10*, 196–215.
53. Boggs, J. M., Rangaraj, G., Heng, Y.-M., and Harauz, G. (2009) Myelin Basic Protein Binds Microtubules to a Membrane Surface *in Vitro*: Effect of Phosphorylation and Deimination. *J. Neurochem. 108* (Suppl. 1), 64.
54. Majava, V., Petoukhov, M. V., Hayashi, N., Pirila, P., Svergun, D. I., and Kursula, P. (2008) Interaction between the C-Terminal Region of Human Myelin Basic Protein and Calmodulin: Analysis of Complex Formation and Solution Structure. *BMC Struct. Biol. 8*, 10.
55. Bates, I. R., Boggs, J. M., Feix, J. B., and Harauz, G. (2003) Membrane-Anchoring and Charge Effects in the Interaction of Myelin Basic Protein with Lipid Bilayers Studied by Site-Directed Spin Labeling. *J. Biol. Chem. 278*, 29041–29047.
56. Homchaudhuri, L., De Avila, M., Nilsson, S. B., Bamm, V. V., Musse, A. A., Smith, G. S. T., Harauz, G., and Boggs, J. M. (2010) SDSL-EPR Study of a C-Terminal Segment of Myelin Basic Protein in a Myelin Mimetic Environment, 54th Annual Biophysical Society Meeting, San Francisco, CA.